T_r = reduced temperature
V = molal volume

LITERATURE CITED

1. Benedict, M., G. B. Webb, L. C. Rubin, and L. Friend, *Chem. Eng. Progr.*, **47**, 419, 449, 571, 609 (1951).
2. Chao, K. C., and J. D. Seader, *AIChE J.*, **7**, 598 (1961).
3. Eckert, C. A., and J. M. Prausnitz, *ibid.*, **11**, 886 (1965).
4. Edmister, W. C., "Applied Hydrocarbon Thermodynamics," Gulf Publishing Co., Houston, Tex. (1961).
5. Hildebrand, J. H., and R. L. Scott, "The Solubility of Non-Electrolytes," 3rd edit., Reinhold, New York (1950).
6. Lee, B. I., and W. C. Edmister, *Ind. Eng. Chem. Fundamentals*, **10**, 32 (1971).
7. *Ibid.*, **10**, 229 (1971).
8. Natural Gas Processors Assoc., Tulsa, Okla., "K and H Computer Program," IBM Ser. 360.
9. Prausnitz, J. M., and P. L. Chueh, "Computer Calculations for High Pressure Vapor-Liquid Equilibria," Prentice-Hall, Englewood Cliffs, N. J. (1968).
10. Prausnitz, J. M., W. C. Edmister, and K. C. Chao, *AIChE J.*, **6**, 214 (1960).
11. Redlich, O., and A. T. Kister, *Ind. Eng. Chem.*, **40**, 345 (1948).
12. Redlich, O., and J. N. S. Kwong, *Chem. Rev.*, **44**, 233 (1949).
13. Starling, K. E., in *Proc. 49th Ann. Conv. Natl. Gas Proc. Assoc.*, Denver (Mar. 1970).
14. Wohl, K., *Trans. AIChE*, **42**, 215 (1946).
15. Yarborough, L., and J. L. Vogel, *Chem. Eng. Progr. Symp. Ser. No. 81*, **63**, 1 (1967).
16. Zudkevitch, D., G. M. Schroeder, and J. Joffe, in "Distillation," Vol. 1, p. 141, Chem. Eng., London (1969).

Manuscript received December 11, 1970; revision received February 18, 1971; paper accepted March 11, 1971. Paper presented at AIChE Houston meeting.

Flow of Viscoelastic Fluids Through a Rectangular Duct

CHANG DAE HAN

Department of Chemical Engineering
Polytechnic Institute of Brooklyn, Brooklyn, New York 11201

A study is carried out on the flow of polymer melts in a rectangular duct. As the theoretical study a three-constant Oldroyd model is used to derive expressions which correlate the rheological properties of materials with the distributions of wall shear rates and wall normal stresses in the rectangular duct. As the experimenal study, a die of rectangular cross section having an aspect ratio of 6 is designed, and then melt extrusion experiments are performed with high density polyethylene. In the experiments wall normal stresses are measured along two adjacent walls of the rectangular duct as a funcion of the axial position. The measurements permit one to obtain the normal stress differences at the duct exit, and then to calculate the distributions of shear rates at two adjacent walls of the rectangular duct, by use of the theoretically derived expressions. Also measured is the extrudate swell, showing trat more pronounced extrudate swell occurs at the long side of the rectangular duct than at the short side. This behavior of extrudate swell correlates with the exit pressure measurements at two adjacent walls of the rectangular duct.

Fully developed flow through a circular tube belongs to the class of viscometric flow, and the extensive theoretical and experimental treatments of such flow problems have well been made for both Newtonian and non-Newtonian viscoelastic fluids. On the other hand, flow through a rectangular duct having a finite aspect ratio may be classified as nonviscometric flow in general, and its theoretical treatment is not as simple as that of viscometric flow. It is particularly difficult for non-Newtonian viscoelastic fluids. As a result, very little work has been done on the problems involved in nonviscometric flow of viscoelastic fluids, from a theoretical as well as experimental point of view.

Some attempts have been made in the past to describe steady rectilinear flow of power law fluids through a rectangular duct (*1* to *4*). Since the power law fluid cannot describe the elastic properties of polymer melts, solution of the equations of motion with the power law model does not explain the elastic behavior of a real viscoelastic fluid, for instance, the die swell phenomenon at the exit of a rectangular duct. Therefore attempts at solving the equations of motion with a more realistic viscoelastic model appear to be desirable. Several years ago Rivlin (*5*) and Langlois and Rivlin (*6*) discussed the slow flow of a viscoelastic fluid along a straight, noncircular tube, using the general constitutive equation advanced by Rivlin and Ericksen (*7*), and showed that rectilinear flow is pos-

sible according to the first-, second-, and third-order theories but not according to the fourth-order theory. Recently a few authors (*8* to *10*) have reported their experimental observations of the presence of Langlois and Rivlin's secondary flows in noncircular ducts.

In the present study an analysis is carried out of the flow of polymer melts in a rectangular duct, as an example of a simple nonviscometric flow, by use of a three-constant Oldroyd model. Experiments were also carried out to measure the axial distributions of wall normal stresses along two adjacent walls of the rectangular duct.

THEORETICAL DEVELOPMENT

Much work in the past has been concerned with the description of materials in viscometric flow, and hence various constitutive equations, such as those advanced by Oldroyd (*11*), Rivlin and Ericksen (*7*), the simple fluid theory due to Noll (*12*) and Coleman and Noll (*13*), and the network theory and its extension due to Lodge (*14*) and Spriggs et al. (*15*), have been extensively evaluated in their applications to steady viscometric flow. An area that has been somewhat neglected in the past but would seem to be worthy of study is simple nonviscometric flow.

The equations of motion for steady fully developed rectilinear flow in a rectangular duct may be written as

$$-\frac{\partial p}{\partial z}+\frac{\partial \tau_{xz}}{\partial x}+\frac{\partial \tau_{yz}}{\partial y}=0 \tag{1}$$

$$-\frac{\partial p}{\partial x}+\frac{\partial \tau_{xx}}{\partial x}+\frac{\partial \tau_{yx}}{\partial y}=0 \tag{2}$$

$$-\frac{\partial p}{\partial y}+\frac{\partial \tau_{xy}}{\partial x}+\frac{\partial \tau_{yy}}{\partial y}=0 \tag{3}$$

in a Cartesian coordinate system, which is referred to in Figure 1. The velocity field in this case is given by

$$\left.\begin{aligned} v_x &= 0 \\ v_y &= 0 \\ v_z &= f(x, y) \end{aligned}\right\} \tag{4}$$

In order to solve the equations of motion—Equations (1), (2), and (3), with the velocity field given by Equation (4)—one needs to consider a constitutive equation which describes properly the relationship between components of the stress and rate of strain tensors of a material. In our theoretical development, use is made of a three-constant Oldroyd model (*16*). This model is chosen on the basis of its ability to predict the essential non-Newtonian viscoelastic behavior, both as regards shear-dependent viscosity and normal stress effects in simple shearing flow.

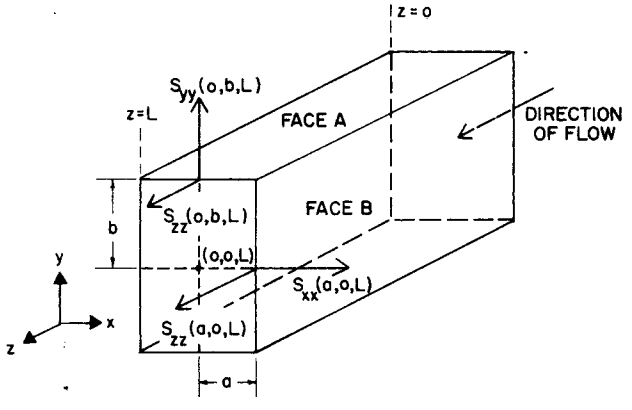

Fig. 1. Schematic representation of rectangular duct.

Williams and Bird (*16*) suggested the three-constant Oldroyd model:

$$(1+\lambda_1 F_0)\tau_{ij}=2\eta_0(1+\lambda_2 F_0)e_{ij} \tag{5}$$

which is a simplified form of the eight-constant Oldroyd model (*11*). In Equation (5) η_0, λ_1, and λ_2 are constants characteristic of the material and τ_{ij} and e_{ij} are ij^{th} components of the stress and rate of strain tensors, respectively. F_0 in Equation (5) is a nonlinear differential operator defined by

$$\begin{aligned} F_0\tau_{ij} &= \frac{\mathcal{D}\tau_{ij}}{\mathcal{D}t}-\tau_{ik}e_{kj}-\tau_{kj}e_{ik}+\frac{2}{3}\tau_{mk}e_{mk}\delta_{ij} \\ F_0 e_{ij} &= \frac{\mathcal{D}e_{ij}}{\mathcal{D}t}-e_{ik}e_{kj}-e_{kj}e_{ik}+\frac{2}{3}e_{mk}e_{mk}\delta_{ij} \end{aligned} \tag{6}$$

in which $\mathcal{D}/\mathcal{D}t$ is the Jaumann derivative (*11*) given by

$$\frac{\mathcal{D}a_{ij}}{\mathcal{D}t}=\frac{\partial a_{ij}}{\partial t}+v_m\frac{\partial a_{ij}}{\partial x_m}-\omega_{im}a_{jm}-\omega_{jm}a_{im} \tag{7}$$

where a_{ij} is the ij^{th} component of a second-order tensor and ω_{im} is the im^{th} component of the vorticity tensor.

For flow in the rectangular duct, as regards Figure 1, the rate of strain tensor is given in Cartesian coordinates by

$$\mathbf{e}=\frac{1}{2}\begin{Vmatrix} 0 & 0 & v_{z,x} \\ 0 & 0 & v_{z,y} \\ v_{z,x} & v_{z,y} & 0 \end{Vmatrix} \tag{8}$$

Use of Equation (8) in Equations (6) and (7) and then in Equation (5) gives

For $i=x,\quad j=x$

$$\tau_{xx}+\frac{\lambda_1}{6}(v_{z,x}\tau_{zx}+4v_{z,y}\tau_{zy})=\frac{2\eta_0\lambda_2}{3}[(v_{z,y})^2-2(v_{z,x})^2] \tag{9}$$

For $i=y,\quad j=y$

$$\tau_{yy}+\frac{\lambda_1}{6}(v_{z,y}\tau_{zy}+4v_{z,x}\tau_{zx}) = \frac{2\eta_0\lambda_2}{3}[(v_{z,x})^2-2(v_{z,y})^2] \tag{10}$$

For $i=x,\quad j=y$

$$\tau_{xy}=-2\eta_0\lambda_2 v_{z,x}v_{z,y} \tag{11}$$

For $i=z,\quad j=z$

$$\tau_{zz}-\frac{4\lambda_1}{3}(v_{z,x}\tau_{zx}+v_{z,y}\tau_{zy})=\frac{2\eta_0\lambda_2}{3}[(v_{z,x})^2+(v_{z,y})^2] \tag{12}$$

For $i=z,\quad j=x$

$$\tau_{zx}-\lambda_1(v_{z,x}\tau_{xx}+v_{z,y}\tau_{xy})=\eta_0 v_{z,x} \tag{13}$$

For $i=z,\quad j=y$

$$\tau_{zy}-\lambda_1(v_{z,x}\tau_{xy}+v_{z,y}\tau_{yy})=\eta_0 v_{z,y} \tag{14}$$

Elimination of τ_{xy} by substituting Equation (11) into Equations (13) and (14) gives

$$\tau_{zx}-\lambda_1 v_{z,x}\tau_{xx}+2\eta_0\lambda_1\lambda_2 v_{z,x}(v_{z,y})^2=\eta_0 v_{z,x} \tag{15}$$

and

$$\tau_{zy} - \lambda_1 v_{z,y} \tau_{yy} + 2\eta_0 \lambda_1 \lambda_2 v_{z,y}(v_{z,x})^2 = \eta_0 v_{z,y} \quad (16)$$

respectively.

Derivation of Wall Shear Rate Expressions

Referring to Figure 1, we have for fully developed flow

$$(v_{z,y})_{a,y} = 0 \quad (17)$$

on face B, indicating that the velocity gradient with respect to the y coordinate is zero along the long side of the rectangle. In a similar fashion, we have on face A

$$(v_{z,x})_{x,b} = 0 \quad (18)$$

along the short side of the rectangle.

Then, use of Equation (17) in Equations (9), (12), and (15) gives

$$(\tau_{xx})_{c,y} + \frac{\lambda_1}{6}(v_{z,x})_{a,y}(\tau_{xx})_{a,y} = \frac{-4\eta_0\lambda_2}{3}(v_{z,x})^2_{a,y} \quad (19)$$

$$(\tau_{zz})_{a,y} - \frac{4\lambda_1}{3}(v_{z,x})_{a,y}(\tau_{zx})_{a,y} = \frac{2\eta_0\lambda_2}{3}(v_{z,x})^2_{a,y} \quad (20)$$

and

$$(\tau_{zx})_{a,y} - \lambda_1(v_{z,x})_{a,y}(\tau_{xx})_{a,y} = \eta_0(v_{z,x})_{a,y} \quad (21)$$

respectively. And use of Equation (18) in Equations (10), (12), and (16) gives

$$(\tau_{yy})_{x,b} + \frac{\lambda_1}{6}(v_{z,y})_{x,b}(\tau_{zy})_{x,b} = \frac{-4\eta_0\lambda_2}{3}(v_{z,y})^2_{x,b} \quad (22)$$

$$(\tau_{zz})_{x,b} - \frac{4\lambda_1}{3}(v_{z,y})_{x,b}(\tau_{zy})_{x,b} = \frac{2\eta_0\lambda_2}{3}(v_{z,y})^2_{x,b} \quad (23)$$

and

$$(\tau_{zy})_{x,b} - \lambda_1(v_{z,y})_{x,b}(\tau_{yy})_{x,b} = \eta_0(v_{z,y})_{x,b} \quad (24)$$

respectively.

Subtracting Equation (19) from Equation (20) and then eliminating $(\tau_{zx})_{a,y}$ in the resulting expression by use of Equation (21) gives

$$(\tau_{zz} - \tau_{xx})_{a,y} = \left[\eta_0\left(\frac{3}{2}\lambda_1 + 2\lambda_2\right) + \frac{3}{2}\lambda_1^2(\tau_{xx})_{a,y}\right](v_{z,x})^2_{a,y} \quad (25)$$

which indicates that the wall shear rates $(v_{z,x})_{a,y}$ can be determined from measurements of the normal stress differences $(\tau_{zz} - \tau_{xx})_{a,y}$ and the deviatoric component of the normal stresses $(\tau_{xx})_{a,y}$ along the long side of the rectangle when flow is fully developed. However, $(\tau_{xx})_{a,y}$ in Equation (25), which is very difficult to measure, if not impossible, can be replaced in terms of the material constants, η_0, λ_1, λ_2, and $(v_{z,x})_{a,y}$, from eliminating $(\tau_{z,x})_{a,y}$ from Equations (19) and (21):

$$(\tau_{xx})_{a,y} = \frac{-\eta_0\left(\frac{\lambda_1}{6} + \frac{4\lambda_2}{3}\right)(v_{z,x})^2_{a,y}}{\left[1 + \frac{\lambda_1^2}{6}(v_{z,x})^2_{a,y}\right]} \quad (26)$$

Now, then, substitution of Equation (26) into Equation (25) gives

$$-(v_{z,x})_{a,y} = \sqrt{\frac{[(\tau_{zz} - \tau_{xx})_{a,y} - A] + \sqrt{[(\tau_{zz} - \tau_{xx})_{a,y} - A]^2 + (\tau_{zz} - \tau_{xx})_{a,y} B}}{C}} \quad (27)$$

where

$$\left.\begin{aligned} A &= 3\eta_0\left(\frac{3}{\lambda_1} + \frac{4\lambda_2}{\lambda_1}\right) \\ B &= -240\eta_0\lambda_2/\lambda_1^2 \\ C &= -20\eta_0\lambda_2 \end{aligned}\right\} \quad (28)$$

Note that the wall shear rate $(v_{z,x})_{a,y}$ in Equation (27) can now be determined from measurements of $(\tau_{zz} - \tau_{xx})_{a,y}$ and from predetermined values of material constants η_0, λ_1, and λ_2.

In a similar manner, the expression of the wall shear rate $(v_{z,y})_{x,b}$ along the short side of the rectangle can be obtained, by use of Equations (22) to (24), as follows:

$$-(v_{z,y})_{x,b} = \sqrt{\frac{[(\tau_{zz} - \tau_{yy})_{x,b} - A] + \sqrt{[(\tau_{zz} - \tau_{yy})_{x,b} - A]^2 + (\tau_{zz} - \tau_{yy})_{x,b} B}}{C}} \quad (29)$$

in which A, B, and C are as defined in Equation (28).

Suppose one now measures the pressures at two adjacent walls at various points in the longitudinal direction (z axis). At some distance downstream in the duct where flow is fully developed, one expects to see a constant pressure gradient in the direction of flow. Referring to Figure 2, for instance, pressure profiles are expected to lie on straight lines in the region where fully developed flow is achieved. When the last pressure measurements are extrapolated to the duct exit, there arises a situation where the extrapolated values of the wall pressure are above the ambient pressure (that is, nonzero gauge pressure). The pressure at the duct exit has been called the exit pressure by the author (*17* to *19*). However, the location of points at which wall pressure measurements are to be taken in a rectangular duct needs some thought. This is because in rectangular ducts the distances from the center of the rectangle to two adjacent walls differ, while in circular tubes the distance is constant to any position on the tube wall from the center of the circle. Hence in rectangular ducts, distributions of the exit pressure are expected to exist along the long and short sides of the rectangle, as schematically shown in Figure 2.

According to Han (*17* to *19*), one has for fully developed flow in a rectangular duct

$$(\tau_{zz} - \tau_{xx})_{a,y} \cong -S_{xx}(a, y, L) \quad (30)$$

along the long side of the rectangle, and

$$(\tau_{zz} - \tau_{yy})_{x,b} \cong -S_{yy}(x, b, L) \quad (31)$$

along the short side of the rectangle. Here, the $S_{xx}(a, y, L)$ are the total wall stresses at the duct exit ($z = L$), acting outward normal to the surface B (referring to Figure 1),

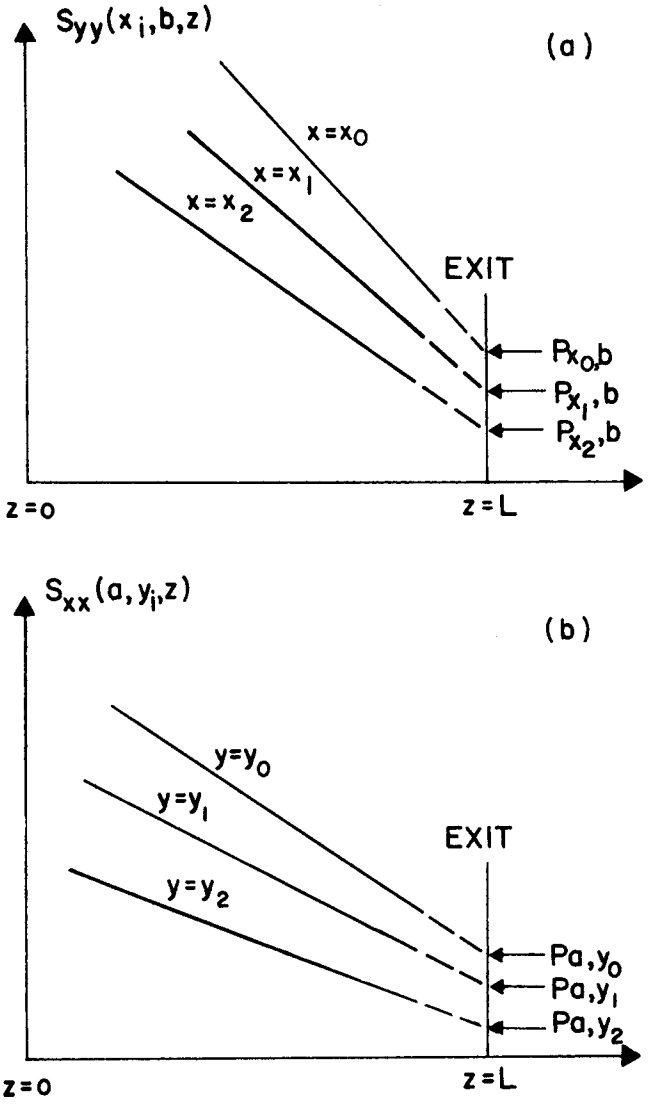

Fig. 2. Schematic representation of the wall normal stress distributions; (a) wall normal stress distributions on face A; (b) wall normal stress distributions on face B.

and the $S_{yy}(x, b, L)$ are the total wall stresses at the duct exit, acting outward normal to the surface A. Note here that

$$S_{ij}(x, y, z) = -p(x, y, z)\delta_{ij} + \tau_{ij}(x, y, z) \quad (32)$$

In the light of Equation (32), it is seen that Equations (30) and (31) imply

$$S_{zz}(a, y, L) \cong 0 \quad (33)$$

and

$$S_{zz}(x, b, L) \cong 0 \quad (34)$$

which has been discussed by the author (*17* to *19*). In other words, the magnitude, at the duct exit, of the normal stresses in the flow direction is negligibly small, at least for polymer melts, compared to the magnitude of the wall normal stresses acting normal to the surfaces.

Since the stresses $S_{xx}(a, y, L)$ and $S_{yy}(x, b, L)$ are compressive, they are related to the exit pressures by

$$-S_{xx}(a, y, L) = P_{a,y} \quad (35)$$

and

$$-S_{yy}(x, b, L) = P_{x,b} \quad (36)$$

Equations (30) and (31) can then be written as

$$(\tau_{zz} - \tau_{xx})_{a,y} = P_{a,y} \quad (37)$$

and

$$(\tau_{zz} - \tau_{yy})_{x,b} = P_{x,b} \quad (38)$$

Now, use of Equation (37) in Equation (27) gives

$$-(v_{z,x})_{a,y} = \sqrt{\frac{(P_{a,y} - A) + \sqrt{(P_{a,y} - A)^2 + P_{a,y}B}}{C}} \quad (39)$$

and use of Equation (38) in Equation (29) gives

$$-(v_{z,y})_{x,b} = \sqrt{\frac{(P_{x,b} - A) + \sqrt{(P_{x,b} - A)^2 + P_{x,b}B}}{C}} \quad (40)$$

It is very interesting to observe from Equations (39) and (40) that the wall shear rates at the long side $(v_{z,x})_{a,y}$ and at the short side $(v_{z,y})_{x,b}$ of the rectangle in rectangular ducts can be determined from measrements of the exit pressures alone, and from the predetermined values of three material constants η_0, λ_1, and λ_2 which are characteristic of the material concerned.

Approximate Velocity Profile

In order to obtain the velocity profile for fully developed rectilinear flow in a rectangular duct, the equations of motion must be solved. It can be easily seen from the above development that use of three-constant Oldroyd model for this purpose gives rise to equations that are very difficult to solve, if not impossible, with some reasonable amount of effort. This is the very reason why very little theoretical work has been done on the subject, except those attempts (*1* to *4*) made using a power law model.

On the other hand, the approach due to Holmes and Vermeulen (*20*) may be taken to obtain the approximate velocity profile:

$$u_z(x, y) = \left\{1 - \left(\frac{x}{a}\right)^m\right\}\left\{1 - \left(\frac{y}{b}\right)^n\right\} \quad (41)$$

The determination of the two constants m and n in Equation (41) then characterizes the velocity profile. One way of determining the values of m and n is by measurements of the velocity gradients at two adjacent walls, as suggested by Holmes and Vermeulen (*20*). However, another way of determining the values of m and n by use of Equations (39) and (40) derived above, without recourse to measurements of the velocity gradient at the wall, is as follows.

Differentiating Equation (41) gives

$$\left(\frac{\partial u_z}{\partial x}\right) = u_{z,x} = -\left(\frac{m}{a}\right)\left(\frac{x}{a}\right)^{m-1}\left(1 - \left(\frac{y}{b}\right)^n\right) \quad (42)$$

and

$$\left(\frac{\partial u_z}{\partial y}\right) = u_{z,y} = -\left(\frac{n}{b}\right)\left(\frac{y}{b}\right)^{n-1}\left(1 - \left(\frac{x}{a}\right)^n\right) \quad (43)$$

Along the long side of the rectangle, where $x = a$, we have

$$(u_{z,x})_{a,y} = -\left(\frac{m}{a}\right)\left(1 - \left(\frac{y}{b}\right)^n\right) \quad (44)$$

and

$$(u_{z,y})_{a,y} = 0 \quad (17)$$

Along the short side of the rectangle, where $y = b$, we

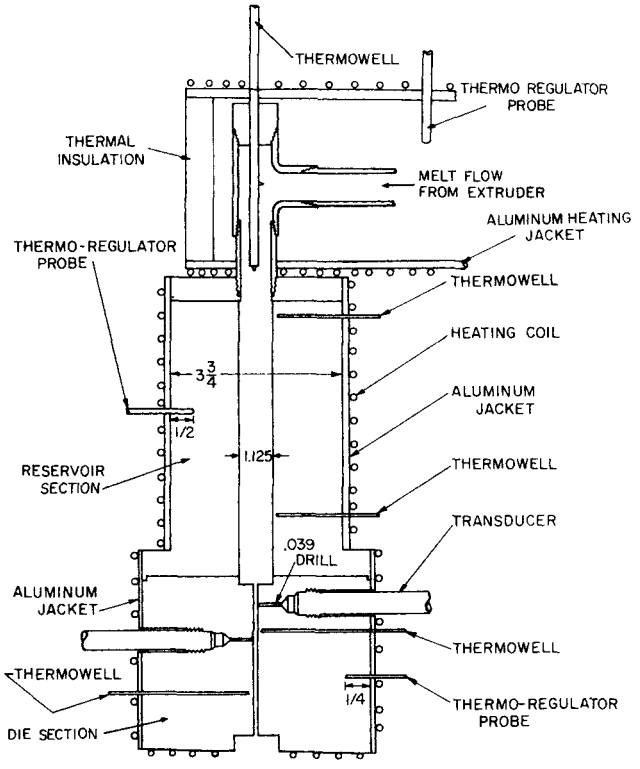

Fig. 3. Design of experimental apparatus.

have

$$(u_{z,y})_{x,b} = -\left(\frac{n}{b}\right)\left(1-\left(\frac{x}{a}\right)^m\right) \qquad (45)$$

and

$$(u_{z,x})_{x,b} = 0 \qquad (18)$$

Now, equating Equation (44) with Equation (39) at $x = a$ and $y = 0$ gives

$$m = \frac{a}{V_m}\sqrt{\frac{(P_{a,0}-A)+\sqrt{(P_{a,0}-A)^2+P_{a,0}B}}{C}} \qquad (46)$$

in which $P_{a,0}$ is the exit pressure at $x = a$ and $y = 0$ (that is, at center of the long side of the rectangle). Therefore measurements of $P_{a,0}$ and V_m will be sufficient to determine the value of m, by use of Equation (46).

In a similar fashion, equating Equation (45) with Equation (40) at $x = 0$ and $y = b$ gives

$$n = \frac{b}{V_m}\sqrt{\frac{(P_{0,b}-A)+\sqrt{(P_{0,b}-A)^2+P_{0,b}B}}{C}} \qquad (47)$$

in which $P_{0,b}$ is the exit pressure at $x = 0$ and $y = b$, (that is, at center of the short side of the rectangle). Hence the value of n can be determined from measurements of $P_{0,b}$ and V_m.

It is then seen from the above that the approximate velocity profile, as given by Equation (41), may be determined from the measurements of the exit pressures and the velocity of the fluid at the center of the rectangle.

EXPERIMENT

Apparatus and Experimental Procedure

Figure 3 shows the apparatus, which consists of an extruder, a reservoir section which connects the outlet of the extruder to the inlet of the die section, and the rectangular die section. Polymer melt flows from the extruder into the reservoir section which is 10 in. long and 1.125 in. diam. From here melt flows into the rectangular slit of the die section. The slit has an aspect ratio of 6, with a short side of 0.1 in. and a long side of 0.6 in. The die is made of a 6-in. long, 5-in. diam. aluminum bar.

Figure 4 gives the detailed layout of the rectangular die section having nine pressure tap holes on the long side and six pressure tap holes along the center of the short side. On the long side three pressure tap holes are located on the center line (2, 4, and 5.5 in., respectively, from the entrance), three (1, 3, and 4.75 in. from the entrance) are 0.1 in. off center, and three (1.469, 2.532, and 3.469 in. from the entrance) are located 0.2 in. off center.

The pressure at the wall (that is, the total radial normal stress) is measured with Dynisco melt pressure transducers. Each pressure transducer is connected to its own d.c. power supply which generates six excitation voltages. The electrical outputs, in millivolts, of the pressure transducers are read on a potentiometer which is balanced with the aid of a d.c. Null Detector. The transducers were calibrated against a dead weight tester and were found to give repeatability to within $\pm 1\%$ of the measured value at pressures of 100 lb./sq. in. gauge and greater. The pressure tap holes at the wall of the rectangular duct have a diameter of 0.039 in.

The temperature is monitored at various positions in the reservoir and die sections with the aid of iron-constantan thermocouples, and the temperature is controlled to within $\pm 0.5°F$. by thermistor-operated thermal regulators. The heating system itself consists of resistance wire wound on aluminum jackets for even distribution and the entire system is well insulated.

Experimental procedure is relatively straightforward. The whole system is first brought up to the desired operating temperature. The extruder is then started, and when the system comes to equilibrium at a given constant flow rate, pressure measurements are taken. Then a new flow rate is set. The volumetric flow rate is determined by collecting the extrudate sample for a certain time interval.

Materials and Operating Conditions

The materials used for the present study were two high density polyethylenes: DMDJ 4309 and DMDJ 5140. These samples have widely different molecular weight distributions and melt indices; DMDJ 4309 has a melt index of 0.2 and a polydispersity of 84, and DMDJ 5140 has a melt index of 0.8 and a polydispersity of 8. All experimental runs were made at a melt temperature of 180°C. Volumetric flow rates were varied from low to high insofar as the capacity of the extruder permitted.

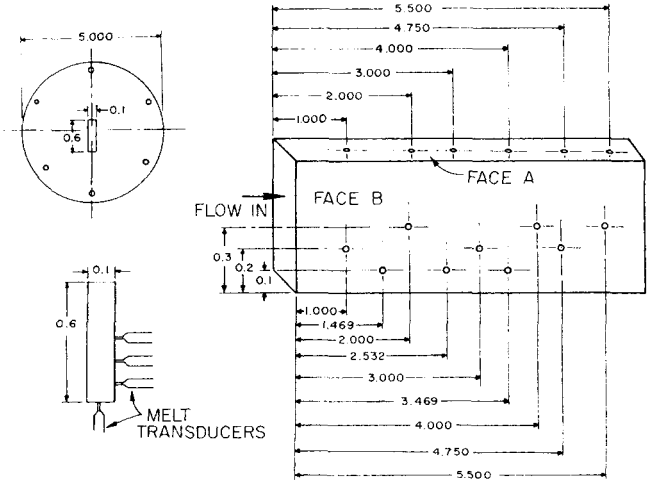

(a) Top view of the slit (b) Layout of the Pressure Tap Holes

Fig. 4. Detailed layout of the location of the pressure tap holes in rectangular duct die (aspect ratio: 6).

RESULTS AND DISCUSSION

Axial Pressure Distribution in Rectangular Ducts

Figure 5 shows typical axial pressure profiles for DMDJ 4309 melts at 180°C., measured at two adjacent walls of the rectangular duct. It is seen from the figure that the pressures measured along the center of the long side of the rectangle lie above those measured along the center line of the short side. Note further that the pressure profiles were obtained at all other flow rates tested, and in Figure 6 are shown the plots of the pressure gradient along the center of the long side versus volumetric flow rate for polyethylene melts at 180°C.

One may consider the plots shown in Figure 6 as equivalent to flow curves (that is, shear stress versus shear rate plots) in circular tubes. However, use of the definition of flow curves is not advisable here, because one does not know how to define shear stress and shear rate in the case of rectangular duct considered here. Furthermore it is to be noted that both the pressure gradient and velocity gradient at the wall vary from position to position along the short side and long side of the rectangle. Yet the plots shown in Figure 6 describe two important facts. First, the pressure gradient versus volumetric flow rate plots follow a power law, suggesting that the fluids tested here were in the non-Newtonian regime. Second, the apparent viscosity of DMDJ 5140 is higher than that of DMDJ 4309. These two facts have already been found by the author (*21*) by use of a circular die. Therefore one can say that the results of the present study are consistent with previous results by the author, so far as viscous properties of the materials tested are concerned.

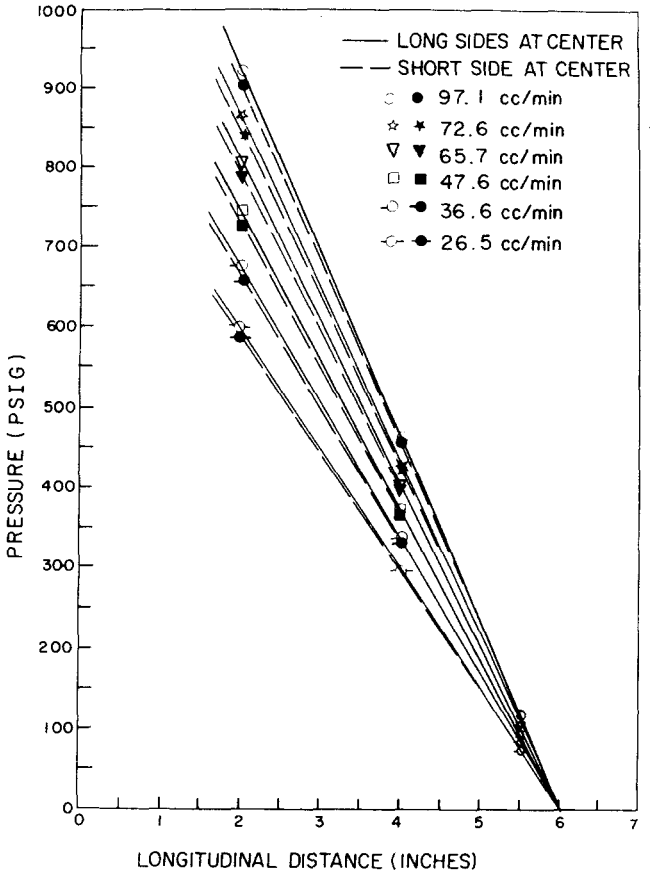

Fig. 5. Plots of axial pressure distributions of DMDJ 4309 melts along the center lines of the long side and short side of the rectangle (T = 180°C.).

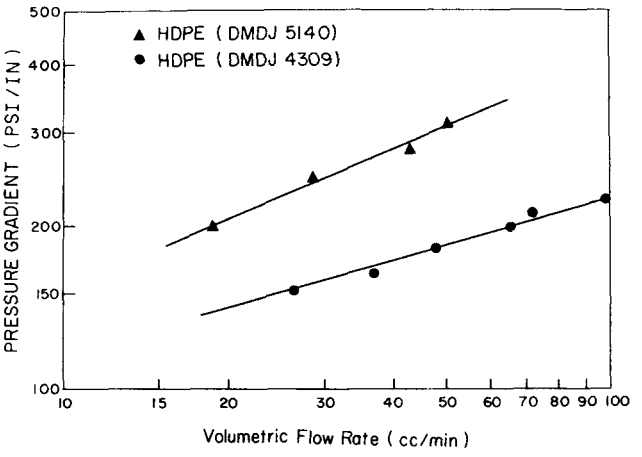

Fig. 6. Plots of pressure gradient versus volumetric flow rate for DMDJ 4309 and DMDJ 5140 melts at center of the long side of the rectangle (T = 180°C.).

Distribution of Normal Stress on the Wall of Rectangular Ducts

The exit pressures were determined by extrapolating the last pressure measurement to the duct exit. This extrapolation may be justified by the constant slope of the pressure profiles (see Figure 5). However, a theoretical argument can be made against the validity of this extrapolation, by virtue of the possible disturbance of the fully developed velocity profile due to exiting. Yet, so far there is no direct experimental evidence to support such argument. The author believes that the possible disturbance to the velocity profiles at the duct exit would be much smaller for polymer melts than for dilute polymer solutions, considering the great difference in magnitude of melt and solution viscosities.

According to the results of the author's previous work (*17, 18*), the extrapolation of the last pressure measurement to the duct exit is expected to give a sizable gauge pressure. Now, a first glance at Figure 5 appears to indicate that the values of the exit pressure in the present study are much smaller than those of earlier studies with circular tubes (*17, 18*). This is however of no surprise to us for the following reasons.

First, the rectangular duct used in the present study has a length-to-thickness (L/h) ratio of 60, which is much larger than the capillary length-to-diameter (L/D) ratios: 4, 8, 12, 16, and 20, used in circular tubes (*17, 18*). This large L/h ratio limited the volumetric flow rate of the polymer melts, because the maximum pressure attainable in the reservoir section is limited by the capacity of the extruder. Second, the previous studies (*17, 18*) of the author have clearly shown that for a given material, the exit pressure increases with shear rate (and hence volumetric flow rate). And for a given flow rate the shear rate in circular tubes increases as the capillary diameter is decreased. The rectangular duct whose cross section is 0.1 in. × 0.6 in. yields a shear rate approximately 20% of that equivalent to circular tubes of 0.125 in. diam.

Therefore, based on these two facts, the apparently small values of the exit pressure shown in Figure 5 are as expected.

Figure 7 shows plots of the exit pressure versus volumetric flow rate for DMDJ 4309, and Figure 8 for DMDJ 5140. Note that the magnitude of the exit pressure at the

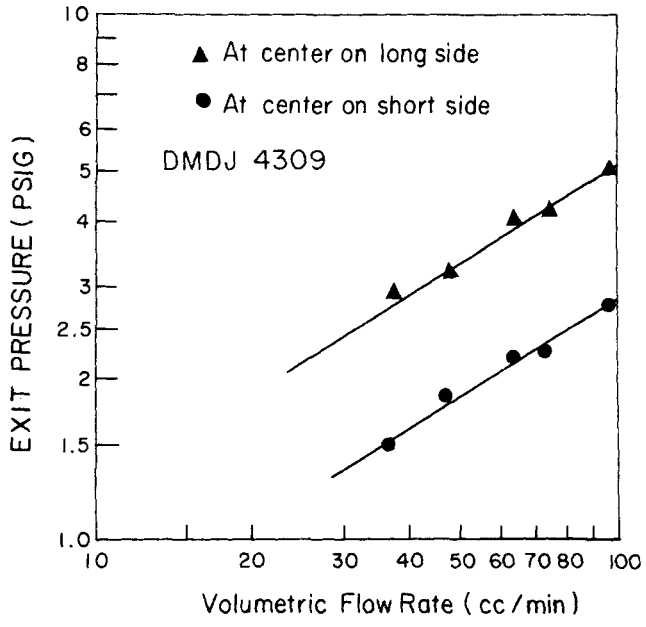

Fig. 7. Plots of exit pressure versus volumetric flow rate for DMDJ 4309 melts ($T = 180°C.$).

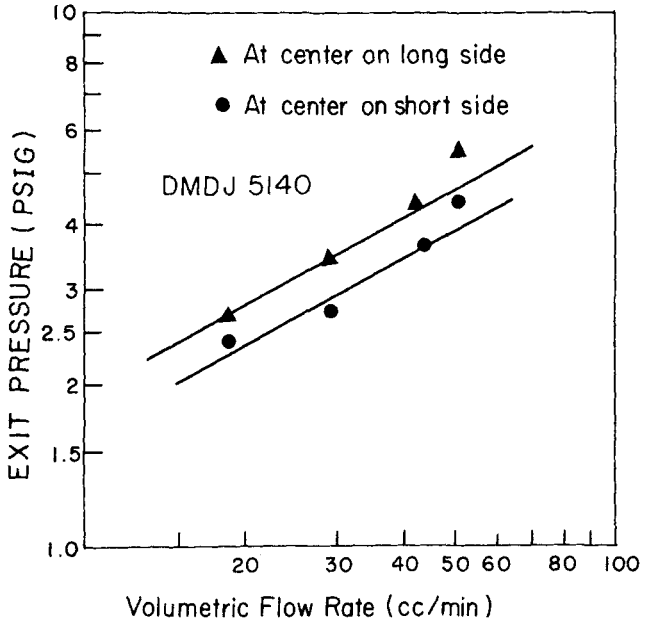

Fig. 8. Plots of exit pressure versus volumetric flow rate for DMDJ 5140 melts ($T = 180°C.$).

center of the long side is greater than that at the center of the short side. Note further that the exit pressure is nothing but the normal stress on the wall [see Equations (35) and (36)] and that the exit pressure is essentially the normal stress difference on the wall, as given by Equations (37) and (38).

It is to be noted that the exit pressures given in Figures 7 and 8 are determined from fitting the linear portions of the pressure profiles by means of the method of least squares. It has been found that the root mean square error of the linear representation of the straight line of the pressure profile did not exceed 0.6 lb./sq.in.gauge.

Now it would be interesting to examine plots of exit pressure versus pressure gradient, which can be prepared by use of Figures 6 and 7 for DMDJ 4309 and Figures 6 and 8 for DMDJ 5140. Such plots are shown in Figure 9 for DMDJ 4309 and DMDJ 5140 melts at center on the long side of rectangle, and in Figure 10 for DMDJ 4309 and DMDJ 5140 melts at center on the short side of rectangle. It is seen from these figures that at the same pressure gradient DMDJ 4309 melts exhibit higher exit pressures than DMDJ 5140 melts. Recently the author (*22*) has suggested a use of the plot of exit pressure versus shear stress as a means of evaluating the relative magnitude of melt elasticity for different materials. Therefore one can conclude from Figures 9 and 10 that DMDJ 4309 is more elastic than DMDJ 5140, which is consistent with the result obtained from the use of a circular die (*21*).

It is appropriate to discuss at this point some of the previous work regarding the distribution of normal stress on the wall of noncircular ducts. Pipkin and Rivlin (*23*)

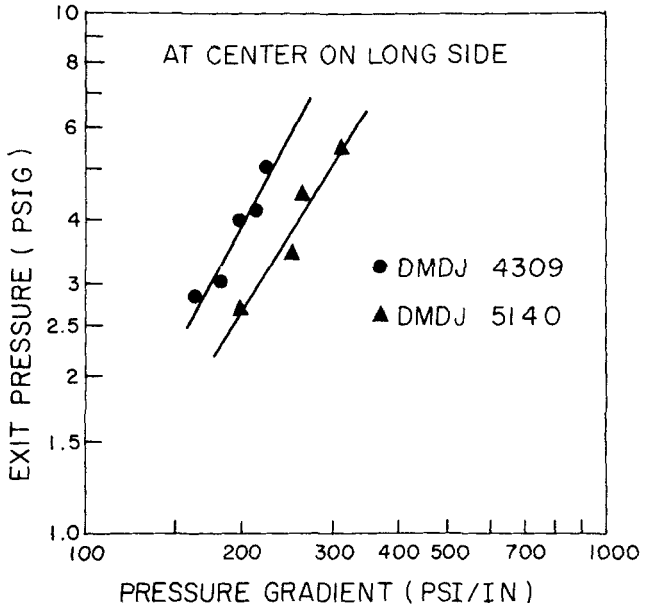

Fig. 9. Plots of exit pressure versus pressure gradient at center on the long side of rectangle for DMDJ 4309 and DMDJ 5140 melts ($T = 180°C.$).

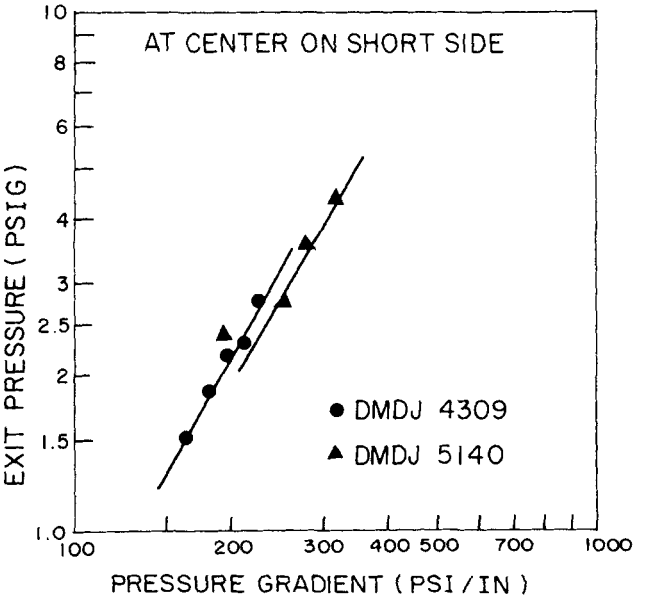

Fig. 10. Plots of exit pressure versus pressure gradient at center on the short side of rectangle for DMDJ 4309 and DMDJ 5140 melts ($T = 180°C.$).

and Pipkin (*24*) pointed out that the distribution of normal stress on the wall of noncircular ducts can be calculated from the first-order perturbation on the solution of the corresponding problem for a Newtonian fluid. More specifically, Pipkin and Rivlin (*23*), in their theoretical development, contended that the normal stresses on the wall can be calculated by taking the normal derivative at the wall of the axial velocity for a Newtonian fluid. Several years ago, Kearsley (*10*) measured the normal stress on the wall of a square duct for polymer solution flow and found that the measured normal stress is distributed nonuniformly on the wall. However, his results have never been published to the author's knowledge.

Extrudate Swell from Rectangular Ducts

The author contended earlier that the exit pressure is a manifestation of the elastic behavior of the material, and further obtained correlations between the exit pressure and extrudate swell in the flow of polymer melts through circular tubes (*17, 18*). In light of the results shown in Figures 7 and 8, one would naturally like to see if there is any correlation between the wall normal stress distributions and the extrudate swell behavior. For this, samples of the extrudate were collected at the same volumetric flow rate as those at which the pressure measurements were taken.

Figure 11 shows photographs of the extrudate cross section of polyethylene melts at 180°C. Two things are worth mentioning about the extrudate swell behavior. First, it has been observed that the extrudate swells more as the volumetric flow rate is increased, which is in accord

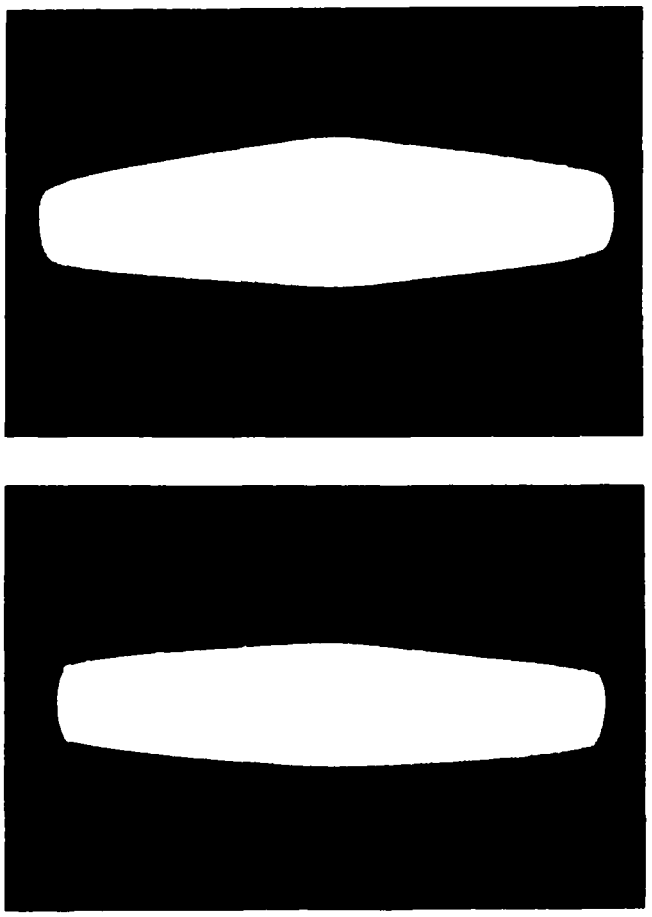

Fig. 11. Extrudate swell behavior: *(top)* DMDJ 4309 at $Q = 72.6$ cc./min., $T = 180$°C.; *(bottom)* DMDJ 5140 at $Q = 52.5$ cc./min., $T = 180$°C.

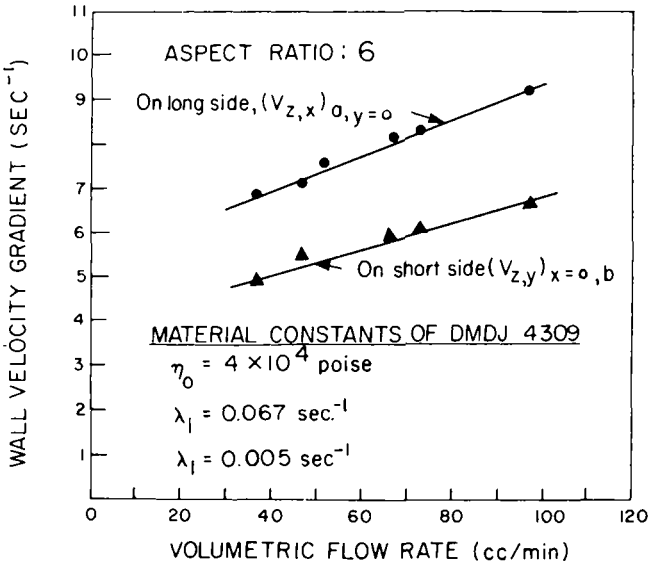

Fig. 12. Calculated wall velocity gradient versus volumetric flow rate plots for DMDJ 4309 melts.

with the observations made in the flow of viscoelastic fluids through circular tubes. Second, more pronounced extrudate swell occurs at the long side of the rectangular duct than at the short side, which is consistent with the distributions of the wall normal stress as shown in Figures 7 and 8. This consistency leads one to the conclusion that the exit pressure is clearly a manifestation of the elastic behavior, which has already been pointed out from the results obtained in the flow through circular tubes.

Wall Shear Rate and Velocity Profile in Rectangular Ducts

Having obtained the exit pressure, one can now calculate wall shear rates by use of Equations (39) and (40). In Figure 12 are shown plots of the wall velocity gradient versus volumetric flow rate, for which the following material constants were used: $\eta_0 = 0.4 \times 10^5$ poise, $\lambda_1 = 0.0668$ sec., $\lambda_2 = 0.005$ sec. These material constants were determined from experimental data, obtained independently with the same material in the flow through circular tubes (viscometric flow), by means of a nonlinear parameter estimation technique, using the expressions relating the shear stress with shear rate and the normal stress difference with shear rate. One can also obtain the velocity profile in the rectangle by use of Equation (41), since the two constants m and n can be determined from Equations (46) and (47) and from the measurement of the exit pressures $P_{a,0}$ and $P_{0,b}$ given in Figures 7 and 8. In Figure 13 are shown the velocity profiles of DMDJ 4309 melts, for which the two constants m and n in Equation (41) are determined from the same experimental data used to constructing Figure 12. It is to be noted that the two constants m and n depend through Equations (46) and (47) on the three material constants η_0, λ_1, and λ_2, of the constitutive Equation (5).

As pointed out earlier, the rigorous approach to obtaining the velocity profile and wall shear rate is to solve the equations of motion, Equations (1) to (3), with the use of the velocity field given by Equation (4), the constitutive equation given by Equation (5), and appropriate boundary conditions. However, to obtain meaningful results, such an approach requires considerable effort mainly due to the complexity of the equations to be solved. In the past, use of power law model has met with some success in giving insight into the velocity profiles in rectangular

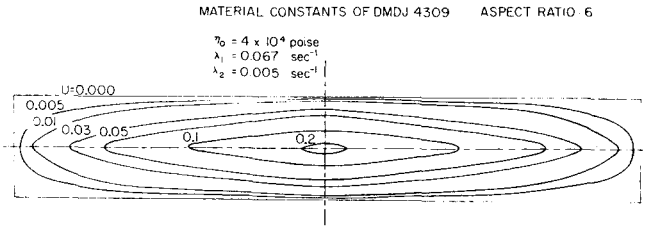

Fig. 13. Calculated velocity profiles for DMDJ 4309 melts.

ducts (*1* to *4*). Although use of the power law model is considerably simpler than that of the three-constant Oldroyd model, insofar as the algebraic manipulation is concerned, obtaining the solution of the equations of motion still requires considerable numerical computation.

In light of the above discussion, the present approach, admittedly yielding approximate velocity profiles, is much simpler, once the measurements of the exit pressures are obtained.

CONCLUSIONS

An experimental technique has been described to carry out a study of the flow of polymer melts through rectangular ducts. Experiment has shown the nonuniform distribution of the wall normal stress at two adjacent walls of the rectangle. The author has then pointed out that the wall normal stresses are essentially the normal stress differences, and that the distribution of the wall normal stresses correlates with that of extrudate swell at two adjacent walls. The similarity between the distributions of the wall normal stress and the extrudate swell is believed to point out the significance of the measurement of the exit pressure. These can then be further used for calculations of wall shear rates and the approximate velocity profiles, which otherwise would be very difficult if not impossible.

For the theoretical work, use of a three-constant Oldroyd model has been made for deriving the expressions of wall shear rate. The expressions contain the normal stress differences on the wall, that is, the wall normal stresses which are measurable from experiment. Having measured the wall normal stresses, the author has calculated the wall shear rates from the theoretically derived expressions. An approach for obtaining the approximate velocity profiles in the flow of polymer melts through rectangular ducts has been presented, which also makes use of the measurements of wall normal stress.

The present study has revealed some insights into a better understanding of the flow behavior of viscoelastic fluids in a simple nonviscometric flow field.

ACKNOWLEDGMENT

The author expresses his gratitude to the Textile Fibers Department, Du Pont de Nemours and Company, for supporting this work.

NOTATION

a = distance from the center to the long side of rectangle (see Figure 1)
b = distance from the center to the short side of rectangle (see Figure 1)
$\mathcal{D}/\mathcal{D}t$ = Jaumann derivative as defined by Equation (6)
e_{ij} = ij^{th} component of the rate of strain tensor
F_0 = nonlinear operator as defined by Equation (6)
h = thickness of the slot ($= 2a$)
L = length of the rectangular duct
m, n = constants in the expression of velocity profile as defined by Equation (41)
p = isotropic pressure
$P_{a,0}$ = exit pressure at center of the long side of the rectangle
$P_{a,y}$ = exit pressure along the long side of the rectangle
$P_{0,b}$ = exit pressure at center of the short side of the rectangle
$P_{x,b}$ = exit pressure along the short side of the rectangle
S_{ij} = ij^{th} component of the total stress tensors
u_z = dimensionless axial velocity profile as defined by Equation (41)
v_x, v_y, v_z = components of velocity
$v_{i,y}$ = ij^{th} component of velocity gradient
x, y, z = rectangular coordinates
V_m = the maximum velocity of the fluid in the rectangle, which occurs at the center of the rectangle

Greek Letters

$\eta_0, \lambda_1, \lambda_2$ = materials constants of the three-constant model given by Equation (5)
τ_{ij} = ij^{th} component of the deviatoric stress tensor
ω_{ij} = ij^{th} component of the vorticity tensor
δ_{ij} = ij^{th} component of the Kronecker delta function

LITERATURE CITED

1. Schechter, R. S., *AIChE J.*, **7**, 445 (1961).
2. Middleman, Stanley, *Trans. Soc. Rheol.*, **9**, 83 (1965).
3. Wheeler, J. A., and E. H. Wissler, *AIChE J.*, **11**, 207 (1965).
4. Arai, T., and H. Toyoda, paper presented at Fifth Intern. Congr. Rheol., Kyoto, Japan (Oct. 1968).
5. Rivlin, R. S., paper presented at Intern. Symp. Second-order Effects in Elasticity, Plasticity and Fluid Dynamics, Haifa, Israel (Apr. 1962).
6. Langlois, W. E., and R. S. Rivlin, *Rend. Math.*, **22**, 1269 (1963).
7. Rivlin, R. S., and J. L. Erickson, *J. Ratl. Mech. Anal.*, **4**, 323 (1955).
8. Giesekus, H., *Rheol. Acta*, **4**, 87 (1965).
9. Wheeler, J. A., and E. H. Wissler, *Trans. Soc. Rheol.*, **10**, 353 (1966).
10. Kearsley, E., private communication.
11. Oldroyd, J. G., *Proc. Roy. Soc.*, **A200**, 523 (1950); **A245**, 278 (1958).
12. Noll, W., *Arch. Ratl. Mech. Anal.*, **2**, 197 (1958).
13. Coleman, B. D., and W. Noll, *ibid*, **6**, 355 (1960).
14. Lodge, A. S., "Elastic Liquids," Academic Press, New York (1964).
15. Spriggs, T. W., J. D. Huppler, and R. B. Bird, *Trans. Soc. Rheol.*, **10**, 191 (1966).
16. Williams, M. C., and R. B. Bird, *Phys. Fluids*, **5**, 1126 (1962).
17. Han, C. D., Marvin Charles, and Wladimir Philippoff, *Trans. Soc. Rheol.*, **14**, 393 (1970).
18. Ibid., **13**, 355 (1969).
19. Han, C. D., and Marvin Charles, *ibid*, **15**, 147 (1971).
20. Holmes, D. B., and J. R. Vermeulen, *Chem. Eng., Sci.*, **23**, 717 1968).
21. Han, C. D., T. C. Yu, and K. U. Kim, *J. Appl. Polymer* Sci., **15**, 1149 (1971).
22. Han, C. D., *AIChE J.*, **16**, 1087 (1970).
23. Pipkin, A. C., and R. S. Rivlin, *Z. Angew. Math. Phys.*, **14**, 738 (1963).
24. Pipkin, A. C., "Proc. Fourth Intern. Congr. Rheol. Part I," E. H. Lee, ed., p. 213, Interscience, New York (1965).

Manuscript received December 22, 1970; revision received March 17, 1971; paper accepted March 19, 1971.